RSC Advances

PAPER

View Article Online
View Journal | View Issue

Cite this: *RSC Adv.*, 2024, **14**, 11877

First-principles study of the mechanical and thermodynamic properties of aluminium-doped magnesium alloys†

Wenjie Zhu,[a] Xingtao Ma,[a] Yarui Wang,*[a] Chaoyong Wang[a] and Wei Li[ab]

Magnesium–aluminum (Mg–Al) alloys are widely used in aerospace, automobile and medical equipment owing to their advantages of easy casting, high strength-to-mass ratio and good biocompatibility. The structural, mechanical, electronic and thermodynamic properties of Mg_xAl_y alloys ($x + y = 16$, $x = 1, 2,\ldots,$ 15) with varying Al-doping contents were studied using the first-principles method. In this work, the structures of Mg_xAl_y alloys were constructed by replacing Mg atoms in a supercell with Al atoms. The lattice parameters of the Al-doped Mg_xAl_y alloys decrease with an increasing Al content because of the smaller atomic size of Al than that of Mg. The calculated formation energies show that $Mg_{11}Al_5$, Mg_5Al_3 and Mg_9Al_7 have prominent structural stability. The analyses of the mechanical properties reveal that the doping of Al improves the ductility of Mg_xAl_y alloys. The elastic moduli increase with an increasing Al content, and Mg_9Al_7 has a notable ability to resist deformation, while $Mg_{11}Al_5$ and Mg_5Al_3 have better plasticity. The calculated results of their electronic properties reveal that $Mg_{11}Al_5$, Mg_5Al_3 and Mg_9Al_7 are good conductors without magnetism. Furthermore, CDD analyses show that the inner layer charges of Al atoms migrated to the outer layer, and the charges of Mg atoms accumulated significantly in the outer region of Al atoms. The Debye temperature of Mg_9Al_7 is higher than that of $Mg_{11}Al_5$ and Mg_5Al_3, indicating that it has better thermodynamic stability. Our findings would be helpful for the design of Mg–Al alloys with excellent mechanical and thermodynamic performances.

Received 18th January 2024
Accepted 27th March 2024

DOI: 10.1039/d4ra00470a

rsc.li/rsc-advances

1. Introduction

Magnesium (Mg) based alloys have the advantages of easy casting, high strength-to-mass ratio and good biocompatibility, which are widely used in fields such as the aircraft industry, automotive production and medical equipment.[1–5] Among all Mg-based alloys, magnesium–aluminum (Mg–Al) alloys hold an important and special position.[6–8] Firstly, the addition of Al could improve the flow ability, hot cracking resistance and mechanical properties of Mg alloys without significantly increasing their density.[9] The density of Mg–Al alloys ranges from 1.74 to 2.7 g cm^{-3}, with a maximum Young's modulus of 78.4 GPa, which has attracted widespread attention in the field of mechanical manufacturing.[10] Secondly, the density and mechanical properties of Mg–Al alloys are close to that of human cortical bones, and they have good biocompatibility and biodegradability.[11,12] These advantages make them extremely suitable as repair materials for human bone injuries. Due to the special applications of Mg–Al alloys, their mechanical, thermodynamic and electronic properties have been extensively studied through experiments.[13–17] For example, Hsu *et al.*[17] prepared several Mg–Al alloy electrodes with different Mg/Al mass ratios using powder metallurgy. They found that the Mg–Al alloy with 75 wt% has the highest efficiency in water electrolysis experiments, considering its anticorrosion property and material costs. Although many studies have been conducted on the properties of Mg–Al alloys, there are still significant challenges in exploring and preparing potential Mg–Al alloys with practical value because of the limitations in experimental equipment and technology. With the development of computer technology and scientific computing software, simulating the properties of materials at the atomic and electron level has become popular. Computational simulation is of great significance for the discovery of new materials and the improvement of material performance through specific designs. Doping other elements or clusters into materials is one of the efficient methods for discovering new high-performance materials, and many valuable works have been done in this regard.[18–23] For example, Abbasi *et al.*[20] studied the effects of elemental doping on the structural and electronic properties of stanene. Their results show that the influence of different

[a]*School of Mathematics and Physics, Henan University of Urban Construction, Pingdingshan 467041, China. E-mail: 20212029@huuc.edu.cn*

[b]*Henan Engineering Research Centre of Building-Photovoltaics, Pingdingshan 467036, China*

† Electronic supplementary information (ESI) available: The mechanical stability criteria and formulas of elastic moduli are listed. Except for $Mg_{11}Al_5$, Mg_5Al_3 and Mg_9Al_7, the elastic constants, elastic moduli and thermal properties of Mg_xAl_y are also given in Tables S1, S2 and S3, respectively. See DOI: https://doi.org/10.1039/d4ra00470a

doping elements on the electronic properties of the structure is significant, which provides a good idea for the design of electronic and optoelectronic devices in the future.

Many factors can affect the mechanical and thermodynamic properties of metal alloys, such as mass ratio, phase composition and grain boundaries.[24–27] Among these factors, the mass ratio of elements in alloys is fundamental and has a significant impact on their performance.[24,25] For Mg–Al alloys, some studies on mass ratios have also been reported.[28–30] Using the atomic substitution method, Zhou *et al.*[28] obtained the supercell of $Mg_{15}Al$ and studied the mechanical and electronic properties. The calculated B/G ratio of pure Mg and $Mg_{15}Al$ are 1.92 and 1.8, respectively, indicating that both structures are ductile. However, computational studies on discovering potential structures of Mg–Al alloys through doping procedures are still very rare. In this work, we aim to screen out potential structures with the lowest energy and stable state from massive initial Mg–Al supercells. Firstly, a large number of Mg–Al supercells with different Mg/Al ratios and substitution sites were constructed using the atomic substitution method. Then, potential stable structures were determined according to formation energies and the convex hull diagram. For the selected structures, we studied their structural features, electronic properties, and mechanical and thermodynamic properties based on density functional theory (DFT) schemes.[31] Our work will provide guidance for designing new Mg–Al alloys and give a further understanding of their structural performance relationships.

2. Methods

The single crystal of Mg belongs to a hexagonal close-packed structure (space group $P6_3/mmc$). As shown in Fig. 1a, each unit cell of Mg contains 2 atoms. The lattice parameters are $a = b = 3.2094$ Å and $c = 5.2105$ Å, which were determined by Batchelder and Raeuchle.[32] A $2 \times 2 \times 2$ supercell with lattice parameters $a = b = 6.4188$ Å and $c = 10.421$ Å was constructed with a total of 16 Mg atoms, as shown in Fig. 1b. The site of each Mg atom can be doped by an Al atom, assuming that the lattice parameters have no change. To study the effect of the Mg/Al ratio on the mechanical and thermodynamic properties of Mg–Al alloys, structures of 15 proportions were constructed according to the formula Mg_xAl_y ($x + y = 16$, $x = 1, 2, \ldots, 15$). For each Mg/Al ratio, the number of the potential structures is C_{15}^{y}, without considering the structural symmetry. Then, optimization calculations were performed on all structures to determine the structure with the lowest energy for each Mg/Al atomic ratio. To further evaluate and determine the stable structures, we calculated the formation energies and convex hull diagram of Mg_xAl_y structures with different Mg/Al ratios.

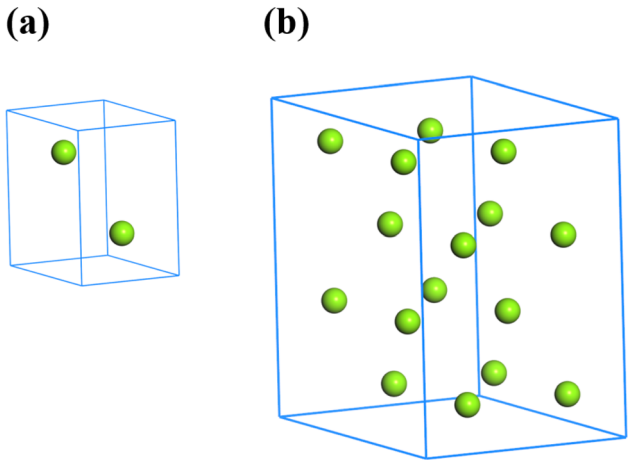

Fig. 1 The unit cell and supercell of Mg.

In this work, all of the calculations were performed using the Vienna *ab initio* simulation package (VASP).[33,34] The generalized gradient approximation (GGA) using the Perdew–Burke–Ernzerhof (PBE) function[35] was used to describe the exchange and correlation interactions, and the projector-augmented wave (PAW)[36,37] method was also used in this work. The kinetic-energy cutoff was set to 500 eV for the plane-wave basis set. All lattice parameters and atomic coordinates were fully relaxed until a force tolerance of 0.01 eV $Å^{-1}$ is reached. The Monkhorst–Pack k-point grids[38] used for all Mg_xAl_y structures are $8 \times 8 \times 12$. The selected parameters ensure that the accuracy of the total energy is converged to within 1.0 meV per atom. The elastic constants were calculated by the stress–strain method.[39] Phonon calculations were carried out using the direct supercell method as implemented in the PHONOPY program[40] to determine the dynamical stability of Mg_xAl_y structures.

3. Results and discussion

3.1 Lattice parameters and formation energies

All optimized structures of Mg_xAl_y with the lowest energy were displayed by the Materials Studio software, as shown in Fig. 2. It is worth noting that the atom number of Mg_xAl_y structures discussed in this paper are all 16, and in order to unify writing standards, x and y are both the simplest ratios. For example, $Mg_{14}Al_2$ is abbreviated as Mg_7Al. The lattice constants, volume and density for Mg_{16}, fcc Al and Mg_xAl_y structures are listed in Table 1. When the number of doped Al atoms is less than 5, the structures with the lowest energy under each Mg/Al ratio show a bias of Al atom aggregation. The results reveal that the doping of Al atoms causes the change of Mg_xAl_y structures, and the values of a, c and c/a fluctuate and show a decreasing trend in general with increasing Al atoms. Due to the smaller atomic radii of Al compared with Mg, the volume of Mg_xAl_y decreases with increasing Al content. In addition, Al has a heavier atomic mass, which leads to an increase in density.

To preliminarily evaluate the stability of the structures, formation energies were calculated and a convex hull diagram was plotted. The formation energy of the Mg_xAl_y structure at 0 K is defined as follows,

$$E_f = (E(Mg_xAl_y) - xE(Mg) - yE(Al))/(x + y) \quad (1)$$

where $E(Mg_xAl_y)$ refers to the total energy of the Mg_xAl_y structure in the ground state, and $E(Mg)$ and $E(Al)$ represent the energy per atom of hcp Mg and fcc Al, respectively.[41] Fig. 3 shows the calculated formation energies and convex hull of Mg_xAl_y structures with different Mg/Al ratios. As depicted in Fig. 3, when the

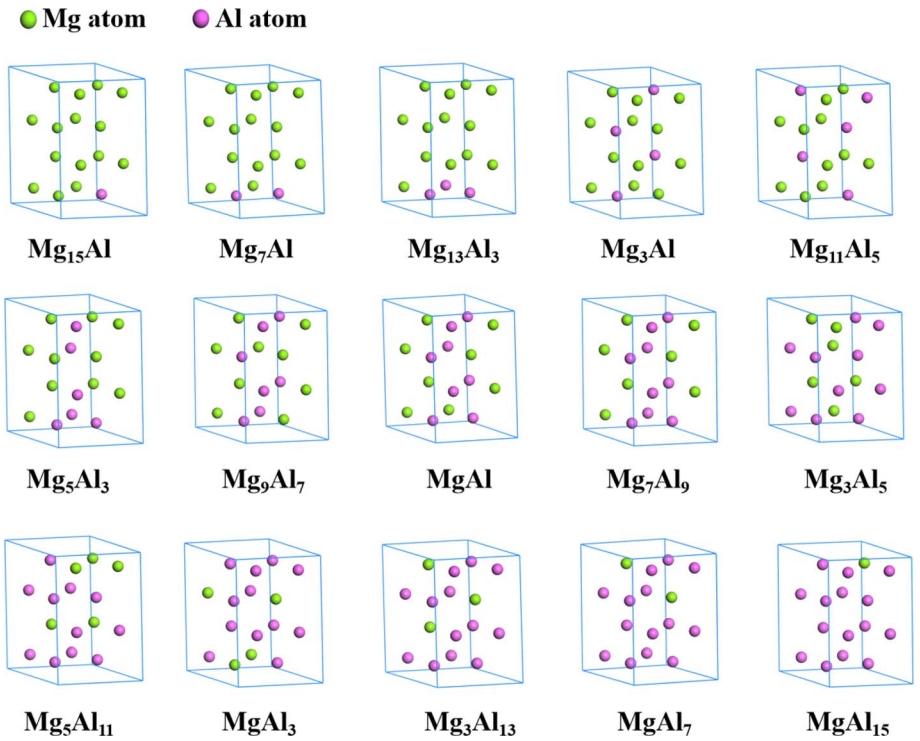

Fig. 2 The structures of Mg_xAl_y with the lowest energy.

Table 1 The lattice constants, volume and density of Mg_{16}, fcc Al and Mg_xAl_y alloys

Structures	a (Å)	c (Å)	c/a	V (Å^3)	ρ (g cm^{-3})
Mg_{16}	6.430	10.39	1.616	365.4	1.745
$Mg_{15}Al$	6.349	10.28	1.619	358.7	1.792
Mg_7Al	6.339	10.24	1.615	351.6	1.842
$Mg_{13}Al_3$	6.233	10.29	1.651	346.0	1.886
Mg_3Al	6.194	10.03	1.619	333.6	1.971
$Mg_{11}Al_5$	6.164	10.02	1.626	327.7	2.022
Mg_5Al_3	6.172	9.936	1.610	321.9	2.074
Mg_9Al_7	6.102	9.772	1.601	314.4	2.140
MgAl	6.056	9.652	1.594	308.8	2.194
Mg_7Al_9	5.998	9.581	1.597	302.4	2.257
Mg_3Al_5	6.043	9.412	1.558	300.0	2.292
Mg_5Al_{11}	6.050	9.403	1.554	295.9	2.341
$MgAl_3$	6.019	9.291	1.544	290.7	2.400
Mg_3Al_{13}	6.013	9.140	1.520	285.9	2.458
$MgAl_7$	5.955	9.142	1.535	281.2	2.516
$MgAl_{15}$	5.893	9.165	1.555	275.7	2.584
Al	4.044			66.17	2.712

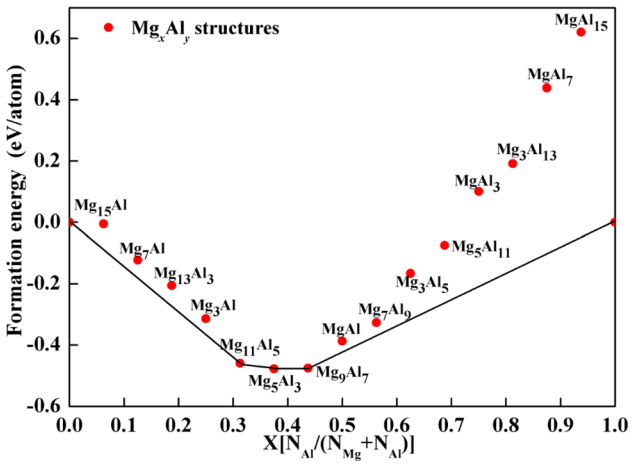

Fig. 3 Calculated formation energy of Mg_xAl_y alloys as a function of Al-doping contents.

number of Al atoms substituted in the Mg_xAl_y structures is greater than 11, the formation energies are positive, indicating that those structures are unstable. Due to the fact that structures with formation energies above the convex hull are metastable,[42] $Mg_{11}Al1_5$, Mg_5Al_3 and Mg_9Al_7 were confirmed to be the most stable structures and adopted for further study.

3.2 Elastic properties

In addition to the formation energy, another index of structural stability is mechanical stability, which can be studied by elastic constants. We calculated the elastic constants of Mg_{16}, fcc Al and Mg_xAl_y structures, as shown in Table 2. For Mg_{16}, the value of C_{11} in this work is 2 GPa smaller than that of Wazzan *et al.*[44] measured through experiments. The values of C_{12} and C_{13} are also very close to the results obtained by Wazzan *et al.* with the largest discrepancy being 3.83%. However, the C_{33} and C_{44} values of Mg_{16} are closer to the results obtained by Slutsky *et al.*[45] through experiments with the largest discrepancy of 3.16%. For fcc Al, the values of C_{11} and C_{12} in this work are very close to those obtained by Le Page *et al.*[39] by *ab initio* calculations with the largest discrepancy of 1.94%, while the value of

Table 2 The elastic constants (GPa) of Mg_{16}, fcc Al and Mg_xAl_y alloys

Structures	C_{11}	C_{12}	C_{13}	C_{33}	C_{44}
Mg[a]	62.4	23.5	22.0	58.9	16.3
Mg[b]	59.5	26.1	21.8	61.6	16.4
Mg[c]	63.5	25.9	21.7	66.5	18.4
Mg_{16}[f]	57.5	27.1	21.0	68.6	18.1
$Mg_{11}Al_5$	70.7	37.5	30.5	79.4	12.9
Mg_5Al_3	73.7	38.5	31.6	80.7	14.5
Mg_9Al_7	76.9	44.6	31.4	88.3	21.6
Al[d]	114.0	62.0			32.0
Al[e]	120.0	61.0			28.0
Al[f]	115.2	63.2			28.9

[a] Ref. 43. [b] Ref. 44. [c] Ref. 45. [d] Ref. 39. [e] Ref. 46. [f] Present work.

C_{44} is 3.1 GPa smaller than theirs. Considering the differences in experimental and computational methods, our calculated elastic constants C_{ij} have a good agreement with their results. Due to the addition of Al, the elastic constants of Mg_xAl_y alloys increase significantly, and the elastic constants of $Mg_{11}Al_5$, Mg_5Al_3 and Mg_9Al_7 increase with increasing Al content. Born's stability criteria[47] is also usually used to determine the mechanical stability of materials. According to Born, any applied strain should increase the energy of the stable ground-state solid. The eigenvalues of the stiffness tensor and its matrix are positive. Therefore, the elastic constants of crystals should satisfy certain conditions according to their symmetry. The formulas of mechanical stability criteria for hcp Mg_{16}, fcc Al and Mg_xAl_y structures are given in ESI.† From our calculated elastic constants, we confirm that Mg_{16}, fcc Al, $Mg_{11}Al_5$, Mg_5Al_3 and Mg_9Al_7 are mechanically stable.

Based on elastic constants, we also calculated the bulk modulus B, shear modulus G and Young's modulus E of Mg_{16}, fcc Al and Mg_xAl_y structures, as shown in Table 3. The elastic moduli and Poisson's ratio v were obtained using the Voigt–Reuss–Hill averaging scheme,[48–50]

$$B = (1/2)(B_R + B_V) \quad (2)$$

$$G = (1/2)(G_R + G_V) \quad (3)$$

$$E = 9BG/(3B + G) \quad (4)$$

$$v = (3B - 2G)/[2(3B + G)] \quad (5)$$

Table 3 The elastic moduli (GPa) of Mg_{16}, fcc Al and Mg_xAl_y alloys

Structures	E	B	G	v	B/G	A^U	H_v
Mg[a]	46.5	35.4	18.1	0.28	1.96		
Mg[b]	44.5	36.6	17.2	0.29	2.06		
Mg_{16}[c]	45.6	35.7	17.7	0.29	2.02	0.12	3.2
$Mg_{11}Al_5$	43.6	46.4	16.2	0.34	2.86	0.27	2.0
Mg_5Al_3	46.6	47.9	17.4	0.34	2.75	0.19	2.2
Mg_9Al_7	53.9	50.8	20.4	0.32	2.49	0.24	2.8
Al	74.6	80.5	27.7	0.35	2.91	0.01	2.9

[a] Ref. 43. [b] Ref. 44. [c] Present work.

where B_R and B_V represent the bulk moduli with the Reuss and Voigt averaging scheme, respectively. G_R and G_V represent the shear moduli with the Reuss and Voigt averaging scheme, respectively. The formulas for calculating B_R, B_V, G_R and G_V through C_{ij} are also given in ESI.† For Mg_{16}, the value of Young's modulus E is 45.6 GPa, which is 0.9 GPa smaller than the value calculated by Velikokhatnyi *et al.*[43] by first-principles calculations and 1.1 GPa larger than the result measured by Wazzan *et al.*[44] through experiments. The bulk modulus B of Mg_{16} is 35.7 GPa, which is very close to the value calculated by Velikokhatnyi *et al.* However, the discrepancy is 2.52%, compared with the result from Wazzan *et al.*. In addition, the shear modulus G of Mg_{16} is 17.7 GPa, which differs from the values of Velikokhatnyi *et al.* and Wazzan *et al.* by 0.4 and 0.5 GPa, respectively. In general, our results are very close to the values obtained by others through experiments and calculations, indicating that the method used in this work to calculate elastic properties is appropriate. For Mg_xAl_y, the elastic moduli increase with increasing Al content. It should be noted that E and G of $Mg_{11}Al_5$ and Mg_5Al_3 have similar values as Mg_{16}, while the bulk moduli B are larger. The doping of Al atoms changes the structure of the Mg supercell, and the results reveal that the effect of Al doping on the volume compression is greater than that of shear and tension. The elastic moduli of Mg_9Al_7 are significantly higher than those of $Mg_{11}Al_5$ and Mg_5Al_3, which is mainly because the Al atoms in Mg_9Al_7 supercell are more concentrated. B/G value can be used to characterize the ductility and brittleness of materials. According to the Pugh criterion,[51] B/G values greater than 1.75 indicate ductility, while a value less than 1.75 characterizes brittleness. Our calculated B/G values show that Mg_xAl_y alloys have better ductility than pure Mg. In addition, the elastic moduli of $Mg_{11}Al_5$, Mg_5Al_3 and Mg_9Al_7 increase with increasing Al content, while the B/G values show an opposite trend. The results indicate that Mg_9Al_7 has the best ability to resist deformation, while $Mg_{11}Al_5$ and Mg_5Al_3 have better plasticity.

The elastic anisotropy of these structures was also studied according to a universal index of $A^U = 5G_V/G_R + B_V/B_R - 6$, which is related to the occurrence of micro-cracks in materials.[52] The departure of A^U from zero (for isotropic crystal) defines the extent of crystal anisotropy and accounts for both the shear and the bulk contributions.[53] As shown in Table 3, the elastic anisotropy index shows that Mg_{16} and Mg_xAl_y structures have considerable elastic anisotropy compared with fcc Al. The A^U value of $Mg_{11}Al_5$ is 0.27, indicating that the anisotropy is the most obvious. In addition, the hardness H_v of these three structures was evaluated according to the empirical correlation,[54]

$$H_v = 0.92(G/B)^{1.137}G^{0.708} \quad (6)$$

where G and B represent the shear modulus and bulk modulus, respectively. Without considering the intercept term, the hardness formula obtained by Chen *et al.*[54] eliminates the possibility of unrealistic negative hardness. For Mg_xAl_y, the hardness of Mg_9Al_7 is larger than that of $Mg_{11}Al_5$ and Mg_5Al_3, as shown in Table 3. Hardness can be regarded as the comprehensive

resistance of chemical bonds to indentation, indicating that the interaction between atoms was enhanced with increasing Al atoms.

3.3 Electronic properties

The electronic properties are of great significance for the development and application of new materials. In this work, we also employed the HSE06 hybrid functional[55] to calculate the electronic band structures of $Mg_{11}Al_5$ (a), Mg_5Al_3 (b) and Mg_9Al_7 (c) with the Fermi level shifted to zero, as shown in Fig. 4. The results reveal that the valence bands and conduction bands of these structures overlap at the Fermi level, resulting in a band gap value of 0. As is well known, conductivity occurs in one or more partially filled energy bands in metals, which possess both valence and conduction band properties. Therefore, our results also confirm that Mg–Al alloy is a good conductor. In addition, we also calculated the magnetization of the structures considering spin polarization. The calculated magnetization values of $Mg_{11}Al_5$, Mg_5Al_3 and Mg_9Al_7 are 0.0029, 0.0028 and 0.0027 A m^{-1}, respectively, which are much lower than the magnetization values of magnetic materials,[56–58] indicating that these structures are in a non-magnetic state.

To discuss the electronic structure of the system further, we also calculated the charge density difference (CDD) for $Mg_{11}Al_5$, Mg_5Al_3 and Mg_9Al_7. The CDD is one of the important ways to investigate electronic structure, which could help us understand the charge transfer induced by the doping of Al atoms. Usually, the charge density of the total system is obtained by subtracting the density of two discrete segments that make it,

$$\Delta\rho = \rho_{(Mg+Al)} - \rho_{(Mg)} - \rho_{(Al)} \quad (7)$$

where $\rho_{(Mg+Al)}$ denotes the total charge density of the Mg_xAl_y structure. $\rho_{(Mg)}$ and $\rho_{(Al)}$ represent the charge densities of Mg and Al fragments taken from the Mg_xAl_y supercell, respectively. As shown in Fig. 5, the yellow and cyan regions represent the positive (electron accumulation) and negative (electron depletion) values, respectively. For $Mg_{11}Al_5$, Mg_5Al_3 and Mg_9Al_7, their CDD exhibits similar charge transfer behavior. The inner layer charges of Al atoms migrated to the outer layer, and the charges of Mg atoms also accumulated significantly in the outer region of Al atoms. Besides, the increase in the charge density at the middle of Al–Al domains reveals the formation of covalent bonds between these atoms. To observe the charge transfer of Al atoms at different sites in the *Z*-direction, two-dimensional cross-sectional color maps at different *z*-positions are also provided. As can be seen from Fig. 5, the charge transfer of Al atoms at different sites is similar; that is, they all migrate outward from the atomic center, with a maximum charge transfer value of $-2.779\ e$ Bohr^{-3}.

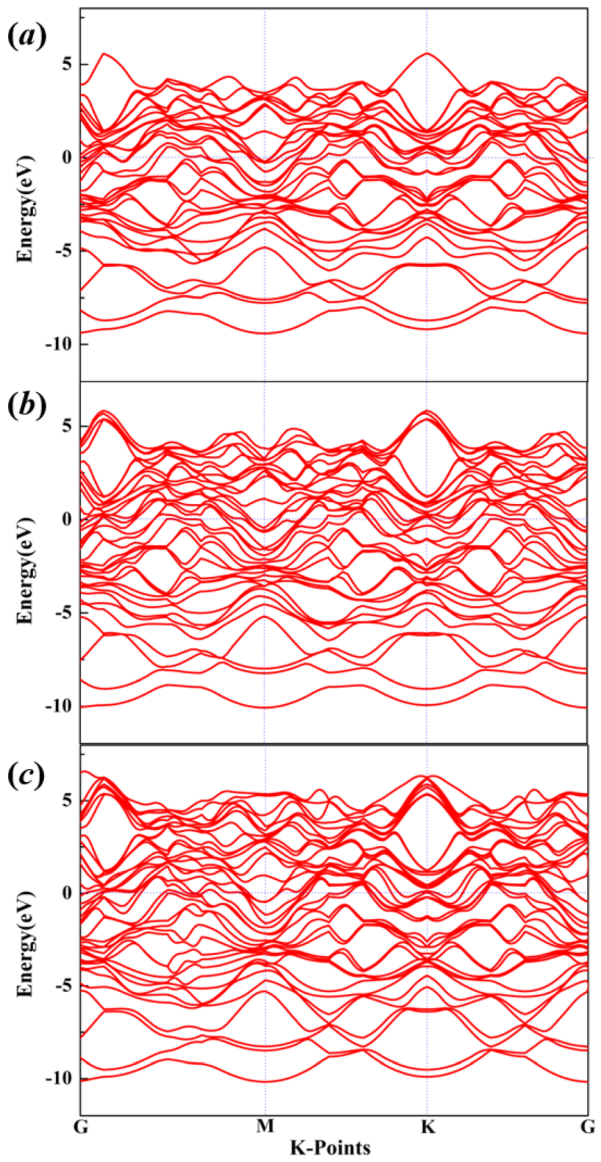

Fig. 4 The electronic band structures of $Mg_{11}Al_5$ (a), Mg_5Al_3 (b) and Mg_9Al_7 (c) with the Fermi level shifted to zero.

3.4 Thermodynamic properties

The Debye temperature (θ_D) is closely related to the elastic constants, melting temperature and specific heat of materials, which can be used to characterize the strength of covalent bonds.[60] In this work, Debye temperature was calculated from the average sound velocity (v_m) as a function of longitudinal sound velocity (v_l) and shear sound velocity (v_t).[60,61]

The calculated θ_D, v_l, v_t and v_m of $Mg_{11}Al_5$, Mg_5Al_3 and Mg_9Al_7 are listed in Table 4. The θ_D value increases with increasing Al content, and the value for Mg_9Al_7 increases by 7.19% compared with Mg_5Al_3. The results reveal that the covalent bond in Mg_9Al_7 is stronger than that of other phases. Hence, the mechanical and thermal stability of Mg_9Al_7 is the best among these three Mg_xAl_y structures, which agrees with the earlier calculated elastic properties. In addition, we further studied the phonon spectrum of the structures, which is another key criterion to characterize the stability of materials.[62] The absence of virtual phonon modes means that the system is dynamically stable. As shown in Fig. 6, the phonon modes for $Mg_{11}Al_5$, Mg_5Al_3 and Mg_9Al_7 in the first Brillouin zone are all real, which is consistent with their negative formation energies

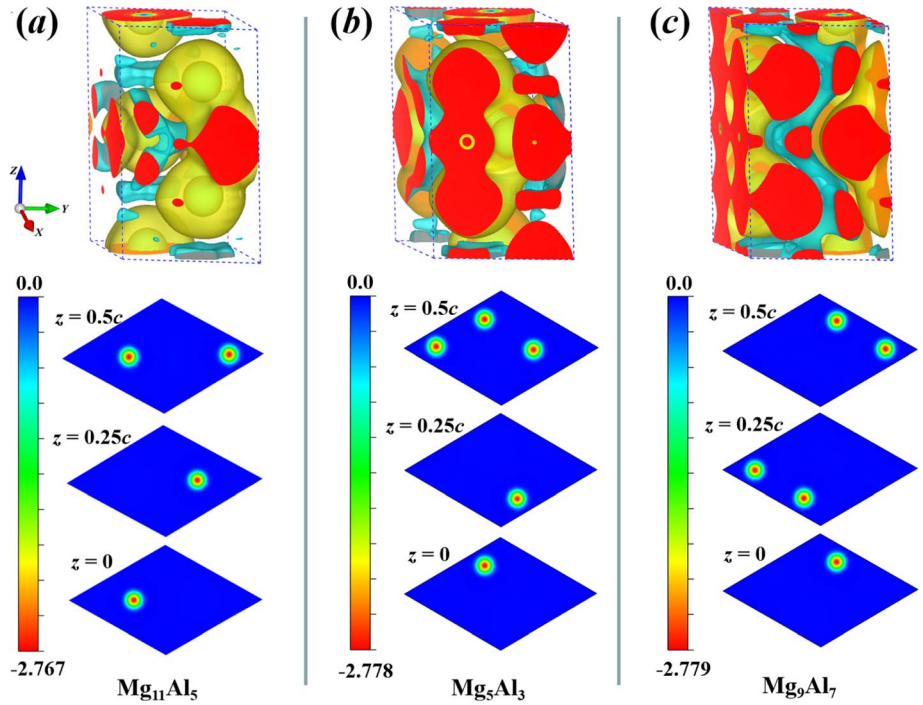

Fig. 5 The charge density difference (CDD) of $Mg_{11}Al_5$ (a), Mg_5Al_3 (b) and Mg_9Al_7 (c) with the isosurface plot level of 0.002 obtained using VESTA software.[59] The yellow and cyan regions represent positive and negative values, respectively. Correspondingly, two-dimensional cross-sectional color maps at different *z*-positions are also provided.

Table 4 Theoretically calculated thermal properties of Mg_xAl_y alloys, including longitudinal sound velocity (v_l), shear sound velocity (v_t), average sound velocity (v_m) and Debye temperature (θ_D)

Structures	v_l (m s^{-1})	v_t (m s^{-1})	v_m (m s^{-1})	θ_D (K)
$Mg_{11}Al_5$	5800.02	2831.13	3180.35	345.99
Mg_5Al_3	5854.61	2896.26	3251.07	355.80
Mg_9Al_7	6035.30	3086.31	3457.53	381.38

and their elastic constants that satisfy Born's criteria. The corresponding phonon density of states (PDOS) was also given in order to visualize the distribution of phonon modes better. Many flat phonon bands were observed, giving rise to sharp peaks in the PDOS plots.

Based on phonon properties, we studied the effect of temperature on heat capacity (C_v), entropy (S) and Gibbs free energy (G) of pure Mg, Al, $Mg_{11}Al_5$, Mg_5Al_3 and Mg_9Al_7. The thermodynamic properties were calculated by PHONOPY software under 0 GPa.[40] As shown in Fig. 7a, the heat capacity C_v increases with increasing temperature and tends to achieve a balance at higher temperatures. In the initial stage (<200 K), Mg and Al show the fastest and slowest increasing speed in C_v with temperature, respectively. The C_v curves of $Mg_{11}Al_5$, Mg_5Al_3 and Mg_9Al_7 are between that of Mg and Al and have similar responses

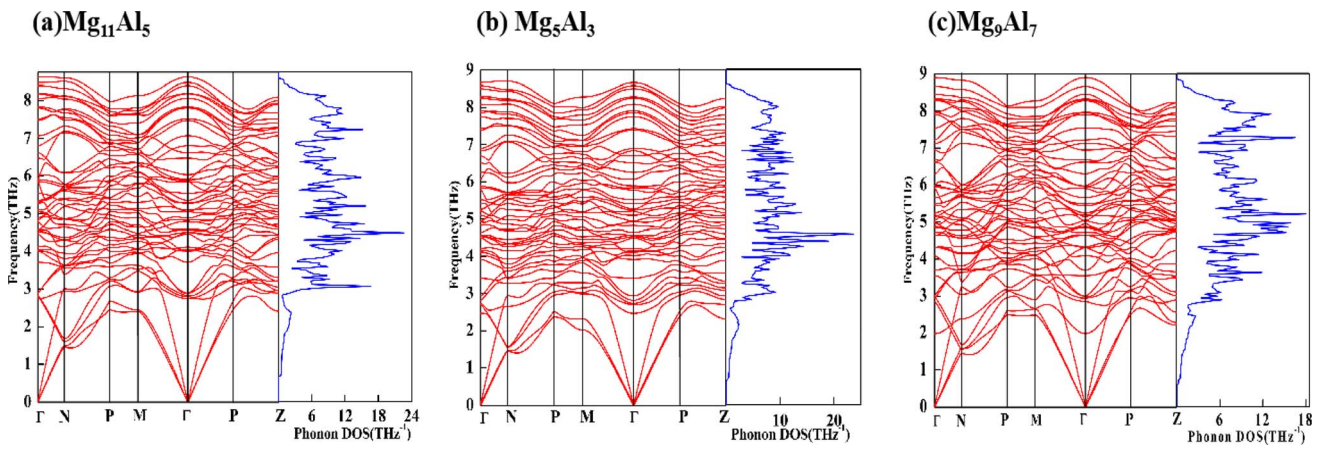

Fig. 6 Phonon spectrum and PHDOS of $Mg_{11}Al_5$, Mg_5Al_3 and Mg_9Al_7.

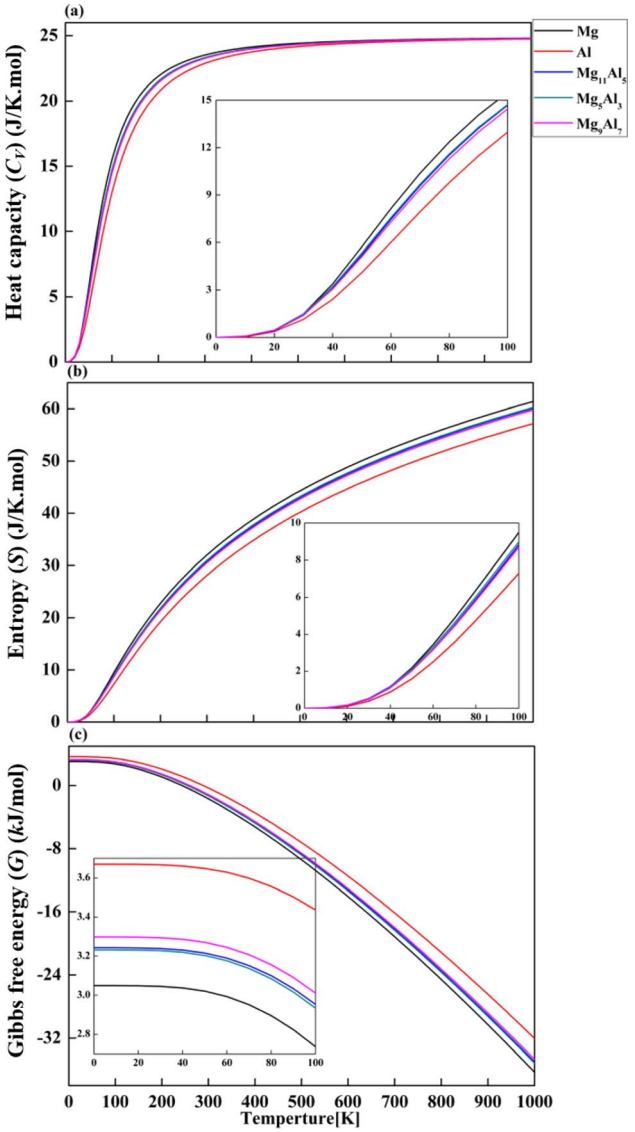

Fig. 7 Thermodynamic properties of (a) heat capacity (C_V), (b) entropy (S) and (c) Gibbs free energy (G) for Mg_{16}, Al and Mg_xAl_y alloys.

to temperature. At about 200 K, the increasing speed of C_v starts to slow down with the change in temperature. After 500 K, C_v changes slightly with temperature and tends to achieve the maximum value of 25 J K^{-1} mol^{-1}. The entropy S increases gradually with increasing temperature, as depicted in Fig. 7b. The entropy of Mg is greater than that of Al in the whole temperature range. The entropy–temperature curves of $Mg_{11}Al_5$, Mg_5Al_3 and Mg_9Al_7 follow the same pattern and have values between that of Mg and Al. From Fig. 7c, it is found that the Gibbs free energy G gradually decreases with increasing temperature. In the whole range of temperature, the values of G obey the following sequence: Al > Mg_9Al_7 > $Mg_{11}Al_5$ > Mg_5Al_3 > Mg.

4. Conclusion

In this work, the structures of Mg_xAl_y alloys ($x + y = 16$, $x = 1$, 2,…, 15) were constructed by atomic substitution method. Structural optimization calculations were performed to determine structures with the lowest energy at each Mg/Al ratio. Their formation energies, elastic moduli, electronic properties and thermodynamic properties were studied using DFT calculations. The lattice parameters of Mg_xAl_y alloys decrease with increasing Al content, which is mainly due to the smaller atomic size of the Al atom compared with that of Mg. According to the convex hull diagram, $Mg_{11}Al_5$, Mg_5Al_3 and Mg_9Al_7 have the best structural stability. The calculated bulk modulus B, shear modulus G, Young's modulus E and Poisson ratio v show that $Mg_{11}Al_5$, Mg_5Al_3 and Mg_9Al_7 have better ductility than pure Mg. Mg_9Al_7 has the largest values of elastic moduli, indicating that it has a better ability to resist deformation. The calculated results of their electronic properties reveal that $Mg_{11}Al_5$, Mg_5Al_3 and Mg_9Al_7 are good conductors without magnetism. Furthermore, the CDD analyses show that the inner layer charges of Al atoms migrated to the outer layer, and the charges of Mg atoms also accumulated significantly in the outer region of Al atoms. The Debye temperature of Mg_9Al_7 is significantly higher than that of $Mg_{11}Al_5$ and Mg_5Al_3, revealing better thermodynamic stability. In terms of mechanical and thermodynamic properties, Mg_9Al_7 is the most promising structure for application. Our computational results would be helpful for the design of Mg–Al alloys and give a further understanding of structure–property relationships.

Author contributions

Wenjie Zhu: data curation, investigation, and writing-original draft, methodology; Xingtao Ma: writing-review and editing, validation; Yarui Wang: writing-review and editing, validation; Chaoyong Wang: writing-review and editing; Wei Li: writing-review and editing. The descriptions are accurate and agreed upon by all authors.

Data availability

The raw/processed data required to reproduce these findings cannot be shared at this time as the data also forms part of an ongoing study.

Conflicts of interest

There are no conflicts of interest to declare.

Acknowledgements

This work was supported by the Natural Science Foundation of Henan Province, the Foundation of Henan Educational Committee (Grant No. 232300420362).

References

1 L. Schlapbach and A. Züttel, *Nature*, 2001, **414**, 353–358.
2 C. Potzies and K. U. Kainer, *Adv. Eng. Mater.*, 2004, **6**, 281–289.

3 Z. B. Sajuri, T. Umehara, Y. Miyashita and Y. Mutoh, *Adv. Eng. Mater.*, 2003, **5**, 910–916.
4 B. Mordike and T. Ebert, *Mater. Sci. Eng., A*, 2001, **302**, 37–45.
5 M. K. Kulekci, *Int. J. Adv. Des. Manuf. Technol.*, 2007, **39**, 851–865.
6 N. C. Goel, J. R. Cahoon and B. Mikkelsen, *Metall. Mater. Trans. A*, 1989, **20**, 197–203.
7 R. J. Nimal, M. Sivakumar, S. G. Raj, S. A. Vendan and G. Esakkimuthu, *Mater. Today: Proc.*, 2018, **5**, 5886–5890.
8 K. Park, J. Park and H. Kwon, *J. Alloys Compd.*, 2018, **739**, 311–318.
9 F. Wang, S. Sun, B. Yu, F. Zhang, P. Mao and Z. Liu, *Trans. Nonferrous Met. Soc. China*, 2016, **26**, 203–212.
10 B. Zheng, L. Zhao, X. B. Hu, S. J. Dong and H. Li, *Physica B*, 2019, **560**, 255–260.
11 F. Peng, H. Li, D. H. Wang, P. Tian, Y. X. Tian, G. Y. Yuan, D. M. Xu and X. Y. Liu, *ACS Appl. Mater. Interfaces*, 2016, **8**, 35033–35044.
12 J. Zou, Z. M. Shi, H. W. Xu and X. L. Li, *BioMed Res. Int.*, 2017, **2017**, 5763173.
13 S. W. Choi, Y. C. Kim, C. S. Kang, J. M. Jung and S. K. Hong, *Adv. Mater. Res.*, 2013, **813**, 427–430.
14 Z. H. Wang, X. L. Zhang, S. B. Li, K. Liu and W. B. Du, *Mater. Sci. Forum*, 2014, **788**, 98–102.
15 S. Maity, A. Sinha and S. Bera, *Nano-Struct. Nano-Objects*, 2018, **16**, 63–68.
16 Z. Jiang, Y. Zhuang, Y. Li and S. Li, *J. Iron Steel Res. Int.*, 2013, **20**, 6–10.
17 W. N. Hsu, T. S. Shih and M. Y. Lin, *Adv. Mater. Sci. Eng.*, 2014, **2014**, 594984.
18 L. W. Huang, O. Elkedim and R. Hamzaoui, *J. Alloys Compd.*, 2011, **509**, S328–S333.
19 Q. Mahmood, G. Murtaza, R. Ahmad, T. Hussain and I. G. Will, *Curr. Appl. Phys.*, 2016, **16**, 361–370.
20 A. Abbasi and J. J. Sardroodi, *Appl. Surf. Sci.*, 2018, **456**, 290–301.
21 A. Abbasi, *RSC Adv.*, 2019, **9**, 16069–16082.
22 A. Abbasi, *Phys. E*, 2019, **108**, 34–43.
23 A. Abbasi, *J. Inorg. Organomet. Polym.*, 2019, **29**, 1895–1915.
24 J. Li, G. Huang, X. Mi, L. Peng, H. Xie and Y. Kang, *Materials*, 2019, **12**, 2855.
25 W. Cheng, L. Tian, Y. Bai, S. Ma and H. Wang, *J. Mater. Res.*, 2017, **32**, 2315–2324.
26 G. Rastelli and E. Cappelluti, *Phys. Rev. B: Condens. Matter Mater. Phys.*, 2011, **84**, 184305.
27 Y. Hu and T. J. Rupert, *J. Mater. Sci.*, 2019, **54**, 3975–3993.
28 L. Zhou, K. Su, Y. Wang, Q. Zeng and Y. Li, *J. Alloys Compd.*, 2014, **596**, 63–68.
29 C. Wang, P. Han, L. Zhang, C. L. Zhang, X. Yan and B. S. Xu, *J. Alloys Compd.*, 2009, **482**, 540–543.
30 P. Volovitch, M. Serdechnova and K. Ogle, *Corrosion*, 2012, **68**, 557–570.
31 W. Kohn and L. J. Sham, *Phys. Rev.*, 1965, **140**, A1133–A1138.
32 F. W. Von Batchelder and R. F. Raeuchle, *Phys. Rev.*, 1957, **105**, 59–61.
33 G. Kresse and J. Furthmüller, *Phys. Rev. B: Condens. Matter Mater. Phys.*, 1996, **54**, 11169–11186.
34 G. Kresse and J. Furthmüller, *Comput. Mater. Sci.*, 1996, **6**, 15–50.
35 G. Kresse and D. Joubert, *Phys. Rev. B: Condens. Matter Mater. Phys.*, 1999, **59**, 1758–1775.
36 P. E. Blöchl, *Phys. Rev. B: Condens. Matter Mater. Phys.*, 1994, **50**, 17953–17979.
37 J. P. Perdew and Y. Wang, *Phys. Rev. B: Condens. Matter Mater. Phys.*, 1992, **45**, 13244–13249.
38 M. Methfessel and A. T. Paxton, *Phys. Rev. B: Condens. Matter Mater. Phys.*, 1989, **40**, 3616–3621.
39 Y. Le Page and P. Saxe, *Phys. Rev. B: Condens. Matter Mater. Phys.*, 2002, **65**, 104104.
40 A. Togo, F. Oba and I. Tanaka, *Phys. Rev. B: Condens. Matter Mater. Phys.*, 2008, **78**, 134106.
41 Y. Q. Wu and M. F. Yan, *Physica B*, 2010, **405**, 2700–2705.
42 R. Arroyave, A. van de Walle and Z. K. Liu, *Acta Mater.*, 2006, **54**, 473–482.
43 O. I. Velikokhatnyi and P. N. Kumta, *Mater. Sci. Eng., B*, 2018, **230**, 20–23.
44 A. R. Wazzan and L. B. Robinson, *Phys. Rev.*, 1967, **155**, 586–594.
45 L. J. Slutsky and C. W. Garland, *Phys. Rev.*, 1957, **107**, 972–976.
46 G. Simmons and H. Wang, *Single Crystal Elastic Constants and Calculated Aggregate Properties*, Cambridge, 1971.
47 M. Born, *Proc. Cambridge Philos. Soc.*, 1940, **36**, 160.
48 W. Voigt, *Lehrbuch der Kristallpysik*, Leipzig, Berlin, 1928.
49 A. Reuss, *Z. Angew. Math. Mech.*, 1929, **9**, 49–58.
50 R. Hill, *Proc. Phys. Soc., London, Sect. A*, 1952, **65**, 349–355.
51 S. F. Pugh, *Relations between the elastic moduli and the plastic properties of polycrystalline pure metals*, Nabu Press, 1954, vol. 45, pp. 823–843.
52 P. Shao, L. P. Ding, D. B. Luo, J. T. Cai, C. Lu and X. F. Huang, *J. Alloys Compd.*, 2017, **695**, 3024–3029.
53 S. I. Ranganathan and M. Ostoja-Starzewski, *Phys. Rev. Lett.*, 2008, **101**, 055504.
54 X. Q. Chen, H. Y. Niu, D. Z. Li and Y. Y. Li, *Intermetallics*, 2011, **19**, 1275–1281.
55 J. Heyd, J. E. Peralta, G. E. Scuseria and R. L. Martin, *J. Chem. Phys.*, 2005, **123**, 174101.
56 N. Shao, J. Li, S. L. Che, J. W. Zheng, L. Qiao, Y. Ying, J. Yu and W. C. Li, *J. Magn. Magn. Mater.*, 2024, **594**, 171476.
57 X. Q. Wu, P. Y. Xu, Y. F. Duan, C. Hu and G. P. Li, *Int. J. Min. Sci. Technol.*, 2012, **22**, 825–830.
58 T. Akune, H. Abe, N. Sakamoto and Y. Matsumoto, *Physica C*, 2003, **388**, 169–170.
59 K. Momma and F. Izumi, *J. Appl. Crystallogr.*, 2011, **44**, 1272–1276.
60 O. L. Anderson, *J. Phys. Chem. Solids*, 1963, **24**, 909–917.
61 P. Wachter, M. Filzmoser and J. Rebizant, *Physica B*, 2001, **293**, 199–223.
62 G. Grimvall, B. Magyari-Köpe, V. Ozoliņš and K. A. Persson, *Rev. Mod. Phys.*, 2012, **84**, 945–986.